Vibration and noise radiation from a panel excited by a turbulent flow

M. Smith and E. Latorre Iglesias

Institute of Sound and Vibration Research, University of Southampton, University Road, S017 1B Southampton, UK
mgs@isvr.soton.ac.uk

Experiments to simulate the flow induced vibration and noise radiation from a car window are described. Two cases are considered: flow over a backwards-facing step and flow over a half-cylinder placed on a flat plate. The first configuration represents the flow separation and subsequent re-attachment into a turbulent boundary layer generated by the A-pillar of a car. The second configuration is representative of the turbulent flow over a side window produced by a car wing mirror. Measurements were carried out in an open jet anechoic wind tunnel at the Institute of Sound and Vibration Research, where a very low noise flow of up to 40 m/s can be achieved. Wall pressure fluctuations were measured using a streamwise array of microphones, from which the Power Spectral Density, coherence and cross-correlation of the pressure fluctuations were obtained. The vibrational response of the test panel was measured on a grid of points and noise radiation was measured using sound intensity mapping and a fixed microphone in the acoustic far-field.

1 Introduction

The noise reduction achieved in cars for noise sources such as the engine, power train and tyres, has in recent years increased the relative importance of aerodynamic noise. Wind noise can be perceptible for velocities of 100 km/h, and may become dominant for velocities higher than 130 km/h. The front side car window is positioned close to the driver's ear and vibrates when excited by the turbulent air flow, so it can be considered as an important source of interior aerodynamic noise.

Many attempts have been made to develop theoretical models of the aerodynamic excitation using CFD (Computational Fluid Dynamics), but the complete process of sound transmission into the car interior must also take account of the coupling of external acoustic waves and convected pressure fluctuations to the window, the dynamics of the window and its sound radiation characteristics. It is considered that the optimal solution to the problem of predicting the sound radiation must be a solution that integrates empirical, experimental and numerical methods [1]. Whilst there have been a number of publications describing measurements of the Wall Pressure Fluctuations (WPF) generated by a Turbulent Boundary Layer (TBL), very little research has been carried out to characterise the other factors in the sound transmission process.

The aim of this research is to measure a high quality set of data that can be used to validate a complete simulation of any such model for the case of a window excited by either a separated flow due to an upstream step or the turbulent wake cause by a 3-D object such as a car door mirror.

2 Experiment Design

The experimental design was a challenging task. First, a facility with low background noise is required. The acoustic energy present in the WPF is several orders of magnitude lower than the energy in the TBL, so acoustic components could easily be masked by background noise. The same masking effect must be avoided during the sound radiation measurements on the receiver side of the test panel. The Institute of Sound and Vibration Research (ISVR) open jet anechoic wind tunnel was used because it provides a high speed flow with very low noise and low turbulence [2] in a free field environment.

Two setups were designed to evaluate the effect of the A-pillar and the wing mirror in the flow. The A-pillar can be approximated as a backwards facing step, this case also being a good benchmark experiment which has been the subject of previous work. For the wing mirror experiment a half cylinder was placed in the flow upstream of a flat panel.

For the WPF measurements the car window was substituted by a "rigid" 8 mm thick Perspex panel. This minimized the effect of panel vibrations on the fluctuating pressures measured, and it was also easy to drill the holes for the microphone array.

For the measurements of vibration and sound radiation of the structure a panel with similar dynamic properties to a standard glass window is necessary in order to obtain relevant data. Evaluating the dispersion curves and coincidence frequency of a standard glass car window 4mm thick and panels of different materials it was found that an aluminum panel 4 mm thick provided very similar performance. Both test panels were fixed in position by screwing them to a frame so as to approximate an idealised zero displacement boundary condition at the edges.

The test panel was surrounded by an acoustic baffle in order to minimised the noise generated by flow interaction with the edges of the panel and also diffraction of sound around the panel. The panel and baffle were not directly connected so as to avoid the transmission of vibration between them. The acoustic baffle was built from a 15mm thick MDF board, covered with a dense acoustic foam on the flow-facing side. This isolated the structure of the baffle from both the acoustic field and the turbulence in the flow. The acoustic baffle was supported by stands clamped to the floor of the chamber to stabilize the whole set-up. Figure 1 shows the front view of the set-up built up for the step and wing mirror cases, where the foam layer of the acoustic baffle can be appreciated (the part of the baffle surrounded the test panel was covered with a thin plastic layer to make it less rough).

For the microphones a small physical size was required, to allow closely spaced measurements, and the effect of the flow on its response had to be considered. Previous work to characterize the dependence of the resolution of the pressure fluctuation under a turbulent boundary layer with the size of the microphone was done by Corcos in 1962 [3]. Subsequents studies revealed a clear tendency to the reduced r.m.s value of the surface pressure with increasing diameter of the microphone [4].

Reducing the size of microphones is difficult, and so the alternative is to place the microphones behind small pin-holes in the test surface. A comparison between pin-holes and flush mounted transducers was made by Bull and Thomas [5]. This pinhole configuration was chosen here in order to reduce the effect of the flow on the transducer membrane, avoiding the distortion due to excessive levels of dynamic and static pressure. Figure 2 shows the details and relevant dimensions of the set-up used.

For the measurements of the WPF an array of transducers with different separation between them is recommended

Figure 1: General view of the experiment set-up for the step case and the wing mirror case.

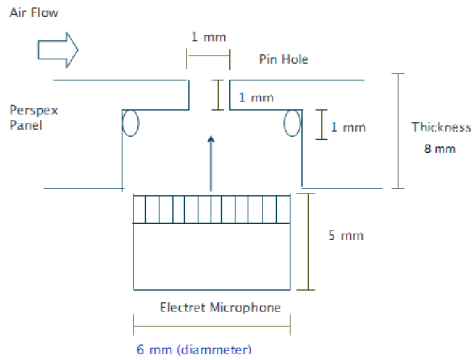

Figure 2: Sketch of the pin holes configuration used for the electret microphones set-up.

by Bremner and Wilby in order that the desired wavenumber components can be captured [1]. Maidanik and Jorgensen proposed a circular platform where a stream-wise line of microphones were flush mounted. By rotating the platform using different angle steps, multiband vector-filters can be obtained even in the span-wise direction [8]. This and other arrangements were used in several other experiments by Arguillat et al., Mein et al. and others [6], [9].

For the tests carried out here a number of linear arrays were specified. One line stretches along the panel in the streamwise direction and three lines cross the panel in the spanwise direction. The length of the array was chosen such that information in the recirculation area, reattachment point and reattached area can be measured. With the design detailed above the minimum achievable distance between microphones is 10 mm so the filter effect between acoustic and convective is expected to be effective up to a maximum frequency of 1120 Hz, this is for a mean flow velocity of 40 m/s to provide the minimum wavelength required in order to avoid spatial aliasing taking into account that the minimum wavelength has to be greater than 2.5 times the distance between microphones. For the acoustic excitation lower spatial resolution is necessary. Calculations were done using Eq. (1) and Eq. (2) where U_c is the convective velocity and λ_{min} is the minimum wavelength required

$$U_c \backsim 0.7 \times U_\infty \tag{1}$$

$$f_{max} = \frac{U_c}{2.5 \times \lambda_{min}} \tag{2}$$

The final design of the array comprised a streamwise line of 75 electret microphones covering the whole length of the panel and three spanwise line arrays at distances of 20 cm, 40 cm and 70 cm from the upstream edge of the panel. The distance between adjacent pinholes is 10 mm.

The calibration of the electret microphones in the array was done by measuring the Frequency Response Function (FRF) between a Gras condenser microphone used as reference and each electret. A broadband noise was generated by a sound source approximately 2m from the array and the reference microphone was positioned adjacent to each electret microphone in turn. In order to calibrate not only the microphone but also the effect of the pin-hole set-up the calibration was done with the electret microphones mounted insitu.

3 Postprocessing and Results

The PSD of the WPF was calculated using Welch's method that gives the average PSD from the Fourier transform of the truncated function $x_T(t)$. Eq. (3) and Eq. (4) considers a signal of length T segmented into q time slices each of them of time T_r (without overlap)

$$\hat{S}_{xx_i}(f) = \frac{1}{T_r}|X^*_{T_{ri}}(f)|^2 \tag{3}$$

$$\tilde{S}_{xx}(f) = \frac{1}{q}\sum_{i=1}^{q}\hat{S}_{xx_i}(f) \tag{4}$$

Figure 3 shows the basic similarity of the PSD for the step and half cylinder cases, though the latter has less low frequency energy and more high frequency energy.

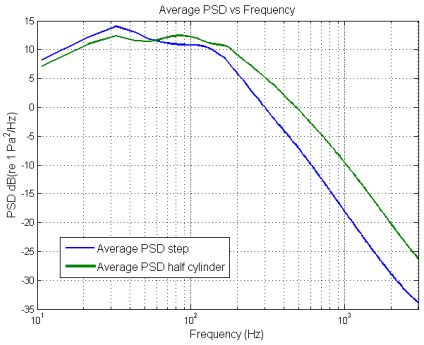

Figure 3: Comparison of the spatial average PSD for the step case and the half cylinder case.

The coherence between different microphones was calculated according to Eq. (5)

$$C_{xy}(f) = \frac{|S_{xy}(f)|^2}{S_{xx}(f)S_{yy}(f)} \tag{5}$$

In this case, signals that were recorded inside the same eddy are expected to be correlated and in consequence the

coherence will be high. If the two microphones are not inside the same eddy then the coherence will be low. Results obtained for coherence evaluated between the position 58 of the streamwise array and positions 59 to 65 are shown in Figure 4

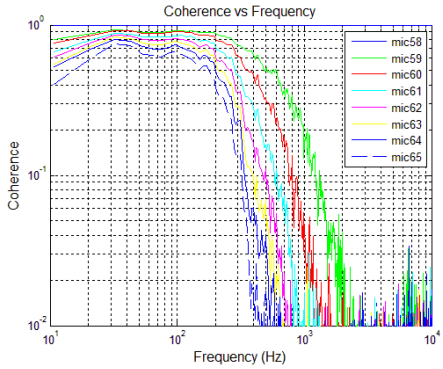

Figure 4: Coherence for the array positions 58 to 65 in the streamwise direction taking microphone number58 as reference, step case.

As expected, the larger the distance between microphones the lower the coherence. Also, a decrease of coherence with increasing frequency is apparent. If the frequency is related with the wavenumber by $U_c = k/\omega$ and the wavenumber is expressed by means its relationship with the wavelength $k = 2\pi/\lambda$ it can be seen how with increasing frequency the length scale of the eddies is reduced. When the length scale is smaller than the distance between two microphones then the coherence between them will be low.

Values of coherence of 0.1 and 0.3 were chosen so for each microphone the particular frequency where these values of coherence were reached were selected. The results obtained are show in Figure 5 for d equals to the distance between microphones (1 cm). It can be seen how the coherence decay is faster when the distance between microphones is bigger.

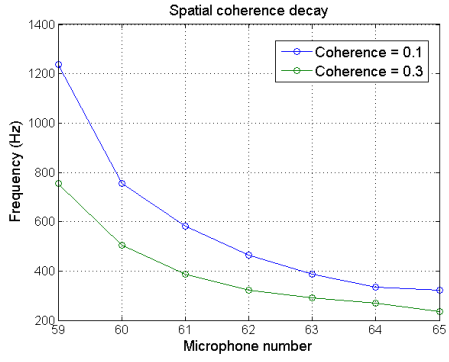

Figure 5: Spatial coherence decay for microphones number 58 to 65 for values of coherence of 0.1 and 0.3 for the step case.

Delays on the arrival of the propagating eddies at different microphones compared with a reference microphones were obtained using the cross correlation function expressed by Eq. (6)

$$\hat{R}_{xy}(m) = \begin{cases} \sum_{n=0}^{N-m-1} x_{n+m} y_n^* & m \geq 0 \\ \hat{R}_{yx}^*(-m) & m < 0 \end{cases} \quad (6)$$

In non-uniform flow the eddies propagate downstream at a convected speed U_c which is less than the free stream velocity. By means of the cross-correlation function the delay between the arrival of the propagating eddy at two different microphones can be detected and from that the convected speed can be calculated. Figure 6 shows the results obtained for the step case taking position 58 of the streamwise array as a reference and evaluation the crosscorrelation between it and positions 59 to 65.

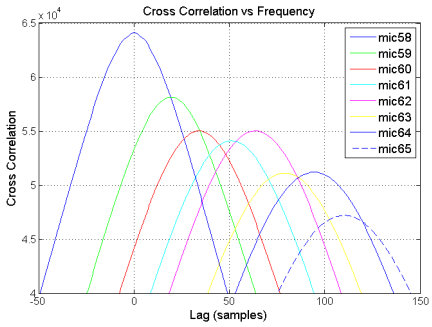

Figure 6: Delay between the microphone number 58 and microphones number 59 to 65 in the arrival of the convected eddies.

The x-axis shows the time lag (in terms of sample number) between the signals. The maximum value of the cross-correlation function corresponds to the lag in the eddy arrival time between the reference microphone and the other microphones evaluated. Then, the number of samples can be converted to time delay by means of equation Eq. (7) where f_s is the sampling frequency used for the data acquisition. The convective speed can then be calculated from the time delay by using equation Eq. (8) where d is the distance between microphones.

$$t_{delay} = lag/f_s \quad (7)$$

$$U_c = d/t_{delay} \quad (8)$$

The convective speed of the propagating eddies in different sections of the streamwise microphone array are gathered in Table 1 for the step and half cylinder cases. For the step case the convective speed increases with distance from the step as the flow is decelerated by the flow separation and reattachment process, then increases again after the reattachment. The same effect is observed for the half cylinder case but this time, for positions close to the obstacle, the convective speed has a negative sign possibly indicating that the recirculating flow is propagating upstream.

The flow induced vibration response of the panel was measured in a grid of 24 points covering the whole panel using a roving accelerometer. Repeatability of the measured data was ensured by using a fixed accelerometer as a reference. Figure 7 shows the response at the 24 points, and also the spatial average of those points. The noticeable peaks that appear in the panel vibration response correspond to the panel modes of vibration being excited by the turbulent flow. The high vibration at very low frequencies is partly due to vibration of the acoustic baffle which was not fully isolated from the test panel in that range.

The sound intensity radiated by the panel was measured by a Microflown p-u intensity probe using the scanning method

Table 1: Propagation speed of the convected eddies in different regions of the microphone array.

Microphones	U_c(m/s)	
	Step	Half Cylinder
1 vs 8	34.3	-10.2
9 vs 16	23.4	-3.7
17 vs 24	24.1	17.2
25 vs 32	24.5	18.3
33 vs 40	24.9	18.6
41 vs 49	25.6	19.3
50 vs 57	27.8	20.7
58 vs 65	28	21.1
66 vs 73	29	21.9

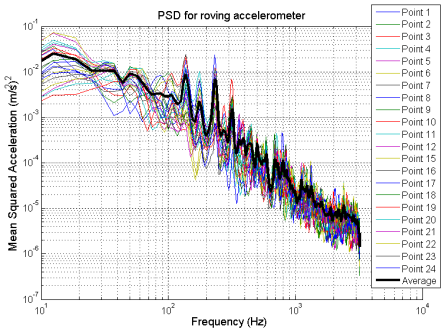

Figure 7: Mean squared acceleration for the 24 points of measurement and spatial average.

called Scan and Paint. First analysis of the measured data showed that sound was leaking through the seal between the test panel and the acoustic baffle. Foam lined barrier material was placed behind these leaks to reduce their effect so the sound radiated by the panel alone could be characterised. A scan of the whole baffle also enabled other weaknesses to be identified. Some low frequency noise from the trailing edge of the baffle still masked the panel noise below 100 Hz but its effect was negligible above this frequency. Figure 8 shows the sound intensity map of the whole structure in the frequency range between 200 Hz and 2 kHz.

The Sound Pressure Level (SPL) radiated by the panel was measured by placing a free-field condenser microphone at a distance of 0.4 m from the panel, simulating the distance between the car window and the driver's ear. Figure 9 shows the SPL radiated by the panel for the step case and the 'background noise' measured with the panel flush mounted with the acoustic baffle (i.e. the noise of the smooth flow TBL is still contributing here). The effect of the step is to increase the noise level by 3 dB across most of the spectrum.

Taking into account that the frequency range chosen is

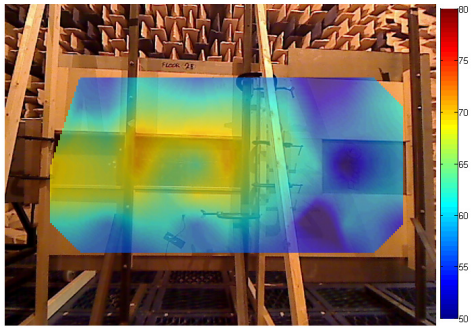

Figure 8: Sound intensity map of the test panel and acoustic baffle in the frequency range between 200 and 2000 Hz for the half cylinder case.

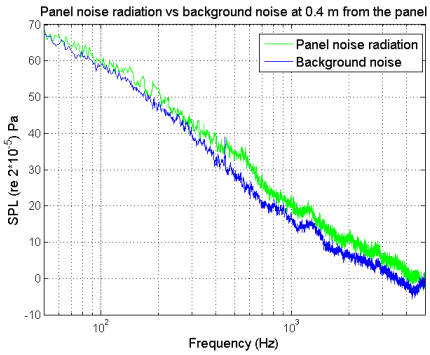

Figure 9: Background noise versus SPLradiated by the panel at 0.4 m from the panel, step case.

above the frequency of the plate's first mode of vibration, and also below the critical frequency of the plate at which the radiation efficiency reaches a peak, the noise radiation in this frequency range is expected to be dominated by the corners and edges of the panel. The results shows in Figure 10 are thus in general agreement expectations.

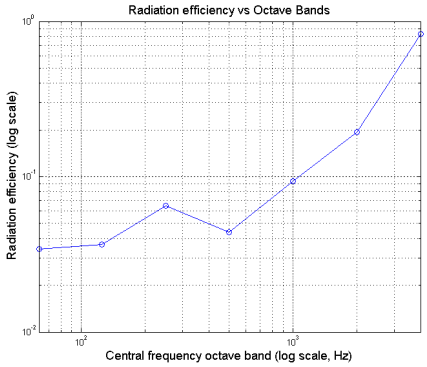

Figure 10: Radiation efficiency in octave bands for the half cylinder case.

The radiation efficiency shown in the previous graph was obtained from the sound power radiated by the panel using Eq. (9) where σ is the radiation efficiency, ρ is the air density, c_0 is the speed of sound and v^2 is the panel surface-average mean squared speed measured by the sound intensity probe in the panel near field.

$$\sigma = \frac{W_r ad}{\rho c_0 S v^2} \tag{9}$$

Figure 11 shows the sound power calculated from the

near-field sound intensity measurements.

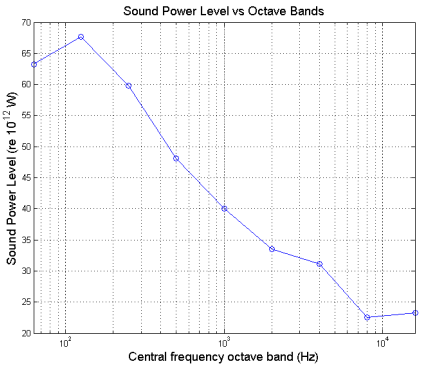

Figure 11: Sound Power level radiated by the panel for the half cylinder case.

4 Conclusion

An experiment to validate a complete aero-vibroacoustic numerical solution for the transmission of flow induced noise of a car window was designed and executed. Two cases were studied: flow over a backward facing step exciting a panel and flow over a half cylinder exciting a panel. The data gathered include the distribution of the wall pressure fluctuations (WPF) over the panel, the vibration response and the sound radiation in the near- and far-field.

Preprocessing of the data showed that a good set of data was obtained. The ISVR open jet anechoic wind tunnel provided a smooth flow with low noise and low turbulence making it possible to achieve the necessary signal to noise ratio. Every part of the experiment was carefully designed: The choice of the microphone array to allow the measurement of the WPF without distortion, with the possibility to spatially filter acoustic and convective excitation below 1120 Hz; The test panel and acoustic baffle were uncoupled to minimise the effect of the baffle vibration response on the test panel. Leakages and weakness in the sound transmission loss of the panel and baffle were detected using sound intensity techniques and corrected using barrier materials.

The WPF results show similar PSDs for the step and half cylinder case but with higher energy in the last case for frequencies above the vortex shedding frequency. Coherence between microphones shows a decay with increasing distance and frequency as expected. The convective speed of the propagating eddies was calculating using crosscorrelation between microphones showing an increase of the speed with distance downstream of the step, and probably a recirculation region close to the half cylinder. Vibration response measured in a grid of 24 points over a aluminum panel shows the panel modes excited by the pressure fluctuations. Near field sound intensity mapping shows a higher radiation coming form the edges and corners of the panel in clear agreement with the expected theoretical results. Moreover, the sound power radiated by the panel was calculated.

Further analysis is proceeding to obtain the decomposition of the acoustic and convective energy of the WPF in the wavenumber-frequency domain and linking the PSD of the WPF with the flow induced panel vibration response and the consequent sound radiation.

Acknowledgments

Thanks to ISVR for allowing to use their facilities to carry out the experiments.

We are very grateful to CD-Adapco who sponsored this project and Fred Mendonca for the support provided.

We also appreciate the technical support given by Paul Bremner and Scott Clifton.

Thanks to Microflown Technologies, particularly to Daniel Fernández Comesaña, for their support in the sound radiation measurements and the lending of the sound intensity scanning equipment.

References

[1] P.G. Bremner,J.F. Wilby, "Aero-vibro-acoustics: Problem statement and methods for simulation-based design solutions", *AIAA conference* **2551**, (2012)

[2] T.P. Chong, P.F. Joseph, P. Davies, "Design and performance of an open jet wind tunnel for aero-acoustic measurement", *Applied Acoustics* **70**(4), 605–614(2009)

[3] G.M. Corcos, "Resolution of pressure in turbulence", *J. Acoust. Soc. Am.* **35**, 192 (1963)

[4] G. Schewe, "On the structure and resolution of wall-pressure fluctuations associated with turbulent boundary-layer flow", *Journal of Fluid Mechanics* **134**(1), 311–328(2004)

[5] M.K. Bull, A.S.W. Thomas, "High frequency wall-pressure fluctuations in turbulent boundary layers", *Physics of Fluids* **19**, 597(1976)

[6] B. Arguillat, D. Ricot, C. Bailly, G. Robert, "Measured wavenumber: Frequency spectrum associated with acoustic aerodynamic wall pressure fluctuations", *J. Acoust. Soc. Am.* **128**(4), 1647–1655(2010)

[7] D.J.J. Leclercq, X. Bohineust, "Investigation and modelling of the wall pressure field beneath a turbulent boundary layer at low and medium frequencies", *Journal of sound and vibration* **257**(3), 477–501(2002)

[8] G. Maidanik, D.W. Jorgensen, "Boundary Wave-Vector Filters for the Study of the Pressure Field in a Turbulent Boundary Layer", *J. Acoust. Soc. Am.* **42**, 494(1967)

[9] M. Mein, F. Dupuy, X. Bohineust, "Experimental characterization of aeroacoustic sources: subsonic flow over a forward-backward step", *AIAA conference*, 2507–2518 (2010)